

Control of sp^2/sp^3 Carbon Ratio and Surface Chemistry of Nanodiamond Powders by Selective Oxidation in Air

Sebastian Osswald,[†] Gleb Yushin,[†] Vadym Mochalin,[†] Sergei O. Kucheyev,[‡] and Yury Gogotsi^{*,†}

Contribution from the Materials Science and Engineering Department and A. J. Drexel Nanotechnology Institute, Drexel University, Philadelphia, Pennsylvania 19104, and Lawrence Livermore National Laboratory, Livermore, California 94550

Received May 11, 2006; E-mail: gogotsi@drexel.edu

Abstract: The presence of large amounts of nondiamond carbon in detonation-synthesized nanodiamond (ND) severely limits applications of this exciting nanomaterial. We report on a simple and environmentally friendly route involving oxidation in air to selectively remove sp^2 -bonded carbon from ND. Thermogravimetric analysis and in situ Raman spectroscopy shows that sp^2 and sp^3 carbon species oxidize with different rates at 375–450 °C and reveals a narrow temperature range of 400–430 °C in which the oxidation of sp^2 -bonded carbon occurs with no or minimal loss of diamond. X-ray absorption near-edge structure spectroscopy detects an increase of up to 2 orders of magnitude in the sp^3/sp^2 ratio after oxidation. The content of up to 96% of sp^3 -bonded carbon in the oxidized samples is comparable to that found in microcrystalline diamond and is unprecedented for ND powders. Transmission electron microscopy and Fourier transform infrared spectroscopy studies show high purity 5-nm ND particles covered by oxygen-containing surface functional groups. The surface functionalization can be controlled by subsequent treatments (e.g., hydrogenization). In contrast to current purification techniques, the air oxidation process does not require the use of toxic or aggressive chemicals, catalysts, or inhibitors and opens avenues for numerous new applications of nanodiamond.

Introduction

Attractive properties of fullerenes and carbon nanotubes (CNTs) explored extensively in the past two decades have triggered a new wave of experimental and theoretical studies on all kinds of nanocarbons.^{1,2} Nanocrystalline diamond, a very promising carbon nanomaterial discovered in the early 1960s in the former Soviet Union, has received much less attention, but the interest in it has been quickly increasing in the past few years.^{3,4} Nanocrystalline diamond can be produced either as thin films using chemical vapor deposition (CVD) techniques or as powder by the detonation of carbon-containing explosives such as trinitrotoluene (TNT) and hexogen in a steel chamber. Both techniques have been the focus of several recent reviews.^{5–8} While nanodiamond films⁷ are undoubtedly attractive as bio-

compatible, smooth, and wear-resistant coatings, it is the nanodiamond powder that has the potential to achieve truly widespread use on a scale comparable to that of CNTs. In this article, we use the term nanodiamond (ND) only for nanodiamond powders produced by the detonation synthesis.

The average diamond particle size in a typical ND is only ~5–8 nm. Due to a large number of unsatisfied surface atoms and a large surface/volume ratio, ND exhibits a very high surface reactivity compared to that of other carbon nanostructures. A new wave of recent interest in ND stems from the expectation that these nanocrystals might be able to combine an active surface, featuring a variety of chemically reactive moieties, with the favorable properties of macroscopic diamonds, including their extreme hardness and Young's modulus, chemical stability, biocompatibility, high thermal conductivity, and electrical resistivity, to name a few. Currently, ND is used in composite materials⁹ as an additive in cooling fluids,¹⁰ lubricants,¹¹ and electroplating baths.⁴ Coarser (100 nm) fluorescent diamond powders may replace quantum dots as fluorescent probes for intracellular processes.¹² A large number of other potential applications, including biocompatible composites, drug delivery, stable catalyst support, chemically resistant chromatographic

[†] Drexel University.

[‡] Lawrence Livermore National Laboratory.

- (1) Shenderova, O. A.; Zhirmov, V. V.; Brenner, D. W. *Crit. Rev. Solid State Mater. Sci.* **2002**, *27*, 227–356.
- (2) Gogotsi, Y. *Carbon Nanomaterials*; CRC Press: Boca Raton, FL, 2006.
- (3) Gruen, D. M.; Shenderova, O. A.; Vul, A. Y. *Synthesis, Properties and Applications of Ultrananocrystalline Diamond*; Springer: Dordrecht, The Netherlands, 2005.
- (4) Dolmatov, V. Y. *Russ. Chem. Rev.* **2001**, *70*, 607–626.
- (5) Shenderova, O. A.; McGuire, G. Nanocrystalline Diamond. In *Nanomaterials Handbook*; Gogotsi, Y., Ed.; CRC Press: Boca Raton, FL, 2006; pp 203–237.
- (6) Danilenko, V. V. *Synthesis and Sintering of Diamond by Detonation*; Energoatomizdat: Moscow, 2003; in Russian.
- (7) Gruen, D. M. *Annu. Rev. Mater. Sci.* **1999**, *29*, 211–259.
- (8) Dolmatov, V. Y. *Ultradisperse diamonds of detonation synthesis: production, properties and applications*; State Polytechnical University: St. Petersburg, 2003.

- (9) Sirotnikin, N. V.; Voznyakovskii, A. P.; Ershova, A. N. *Phys. Solid State* **2004**, *46*, 746–747.
- (10) Davidson, J. L.; Bradshaw, D. T. U.S. Patent 6858157B2, 2005.
- (11) Red'kin, V. E. *Chem. Technol. Fuels Oils* **2004**, *40*, 164–170.
- (12) Yu, S. J.; Kang, M. W.; Chang, H. C.; Chen, K. M.; Yu, Y. C. *J. Am. Chem. Soc.* **2005**, *127*, 17604–17605.

materials with a tailorable surface, transparent coatings for optics,³ and others still remain under-explored. Most of these applications are hindered due to the current inability of the manufacturers to provide ND with well-controlled surface chemistry and the absence of a process that would achieve this control in a research laboratory. Simple calculations show that for ND particles with a diameter less than 5 nm almost 20% of the total number of atoms are on the surface. With further decrease of particle size, this value drastically increases, and properties of ND crystals become mainly determined by their surface.

The raw diamond-bearing soot obtained during detonation synthesis consists of nanodiamond particles, nondiamond carbon, as well as metals, metal oxides, and other impurities coming from the detonation chamber or the explosives used. The purification treatment is the most complicated and expensive stage of the ND production.⁴ Most producers employ wet chemistry approaches to purify ND.³ While these techniques are widely used, they do not provide sufficient purity of ND leading to the black or dark-gray color of commercially available ND powders. In addition, liquid-phase purification is not an environmentally friendly process and requires expensive corrosion-resistant equipment and costly waste disposal processes. Alternative dry chemistry approaches, including catalyst-assisted oxidation,¹³ oxidation using boric anhydride as an inhibitor of diamond oxidation,¹⁴ and ozone-enriched air oxidation,¹⁵ also require the use of either toxic and aggressive substances or supplementary catalysts which result in additional contamination or a significant loss of the diamond phase.

The use of functionalized ND^{15,16} would provide full benefits in most applications only if ND did not contain amorphous or fullerenic carbon shells on the surface and was free of potentially toxic and undesired metal particles incorporated in these shells. Dispersion of strong chemically bonded agglomerates is another major issue limiting the use of ND, and it is also determined by our ability to control the surface of ND particles.

Our recent study of air oxidation of double-wall carbon nanotubes (DWCNT) demonstrated the possibility of selectively removing the amorphous carbon phase without introduction of defects in CNTs.^{17,18} Because the process is simple, inexpensive, environmentally friendly, and scalable, selective removal of nondiamond carbon in the ND soot by air oxidation would be very attractive. However, thus far it has not been considered feasible.¹⁴ In this article, we report on the appropriate air oxidation conditions for purification of ND without a significant loss of the diamond phase.

Materials

The ND used in this study was produced by detonation synthesis and supplied by NanoBlox, Inc. (Boca Raton, FL). Table 1 summarizes selected properties and composition of the three samples (UD50, UD90, and UD98) used in our study. Black UD50 is the raw detonation soot containing nondiamond carbon structures such as amorphous carbon,

carbon onions, fullerenic shells, and graphite ribbons. The black color of the powder is related to the high content of sp² carbon. UD90 and UD98 samples were prepared by different multistage acidic purifications using nitric and sulfuric acids and mainly consist of nanodiamond particles and amorphous carbon (Table 1). In addition to sp² carbon, all powders contain metal impurities, mainly iron (Table 1), often surrounded by carbon shells, as revealed by transmission electron microscopy (TEM).

Methods

Oxidative purification was done under isothermal conditions using a THM600 Linkam heating stage and a tube furnace and under nonisothermal conditions using a thermobalance (Perkin-Elmer TGA 7). Isothermal experiments included two steps: (i) rapid heating at 50 °C/min to the selected temperature and (ii) isothermal oxidation for 5 h in ambient air at atmospheric pressure. The THM600 Linkam heating stage was calibrated by using the melting points of AgNO₃ (209 °C), tin (232 °C), KNO₃ (334 °C), and Ca(OH)₂ (580 °C). In every case, the difference between the measured and expected melting point did not exceed 2 °C. TGA analyses were conducted under a minimal ambient air flow of 40 mL/min in the temperature range between 25 and 800 °C. A heating rate of 1 °C/min was chosen for all experiments.

Characterization

Argon sorption analysis was done using Quantachrome Autosorb-1 at −195.8 °C. The Brunauer–Emmett–Teller (BET) equation¹⁹ was used to evaluate the specific surface area (SSA) of ND.

Raman analysis of the initial and oxidized powders was conducted using a Renishaw 1000/2000 spectrometer with an excitation wavelength of 325 nm (He–Cd laser) in backscattering geometry. In situ Raman studies were performed under 325- and 633-nm (He–Ne laser) excitation. Experimental details related to the in situ measurements have been described elsewhere.^{17,20}

Soft X-ray absorption near-edge structure (XANES) spectroscopy experiments were performed at undulator beamline 8.0 at the Advanced Light Source (ALS) at Lawrence Berkeley National Laboratory (LBNL). Spectra were obtained by measuring the total electron yield by monitoring the total sample photocurrent. The incoming radiation flux was monitored by measuring the total photocurrent produced in a highly transmissive Au mesh inserted into the beam. All XANES spectra were normalized to the Au mesh photocurrent. The monochromator was calibrated by aligning the π* resonance in the carbon K-edge of highly oriented pyrolytic graphite (HOPG) to 285.4 eV. After a linear background subtraction, all spectra were normalized to the post-edge step heights. The relative changes in the sp³-bonded carbon content of ND samples were estimated from XANES spectra using the procedure described in refs 21 and 22 where the relative intensity ratios of π*/σ* states in ND samples and in HOPG (pure sp²-bonded carbon) are compared:

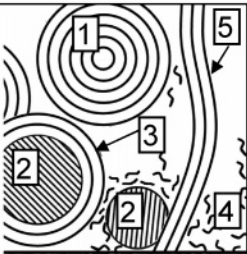
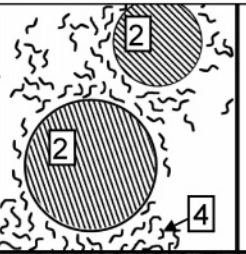
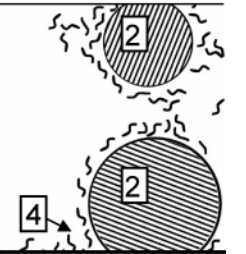
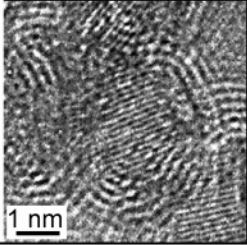
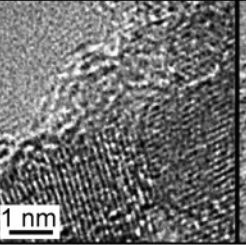
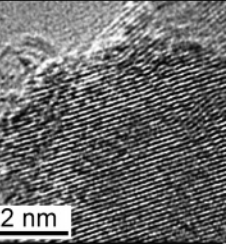
$$\% \text{ sp}^2_{\text{ND}} \approx \frac{(\pi^*/\sigma^*)_{\text{ND}}}{(\pi^*/\sigma^*)_{\text{HOPG}}}; \quad \% \text{ sp}^3_{\text{ND}} = 100\% - \% \text{ sp}^2_{\text{ND}} \quad (1)$$

For the numerical integration, the energy ranges of 282–287 eV and 293–302 eV were used to represent the π* and σ* states' contributions to the XANES spectra. The HOPG spectrum was measured with the

- (13) Gubarevich, T. M.; Sataev, R. R.; Dolmatov, V. Y. In *Chemical purification of ultradisperse diamonds*, 5th All-Union Meeting on Detonation, Krasnoyarsk USSR, Aug 5–15, 1991; Krasnoyarsk USSR, 1991; pp 135–139.
- (14) Chiganov, A. S. *Phys. Solid State* **2004**, *46*, 595–787.
- (15) Li, L.; Davidson, J. L.; Lukehart, C. M. *Carbon* **2006**, *44*, 2308–2315.
- (16) Matrab, T.; Chehimi, M. M.; Boudou, J. P.; Benedic, F.; Wang, J.; Naguib, N. N.; Carlisle, J. A. *Diamond Relat. Mater.* **2006**, *15*, 639–644.
- (17) Osswald, S.; Flahaut, E.; Ye, H.; Gogotsi, Y. *Chem. Phys. Lett.* **2005**, *402*, 422–427.
- (18) Osswald, S.; Flahaut, E.; Gogotsi, Y. *Chem. Mater.* **2006**, *18*, 1525–1533.

- (19) Brunauer, S.; Emmett, P.; Teller, E. *J. Am. Chem. Soc.* **1938**, *60*, 309–319.
- (20) Yushin, G. N.; Osswald, S.; Padalko, V. I.; Bogatyreva, G. P.; Gogotsi, Y. *Diamond Relat. Mater.* **2005**, *14*, 1721–1729.
- (21) Kulik, J.; Lempert, G. D.; Grossman, E.; Marton, D.; Rabalais, J. W.; Lifshitz, Y. *Phys. Rev. B* **1995**, *52*, 15812–15822.
- (22) Gago, R.; Jimenez, I.; Albella, J. M.; Climent-Font, A.; Caceres, D.; Vergara, I.; Banks, J. C.; Doyle, B. L.; Terminello, L. J. *J. Appl. Phys.* **2000**, *87*, 8174–8180.

Table 1. Structure and Selected Physical Properties of the Investigated Samples

	UD50	UD90	UD98
Schematic of carbon structures present in the samples^a			
HRTEM micrograph			
sp³ carbon content^b, %	23	70	81
Ash content^c, wt.%	3.1	2.0	1.3
Fe content^c, wt.%	1.3	0.7	0.2
BET-SSA, m²/g	460	367	350

^a – as determined using TEM notation used in the schematics: (1) - carbon onion, (2) - nanodiamond, (3) - fullerene shell, (4) - amorphous carbon, (5) – graphite ribbon

^b – as determined using XANES

^c – as reported by the supplier

^a As determined using TEM. Notation used in the schematics: (1) carbon onion, (2) nanodiamond, (3) fullerene shell, (4) amorphous carbon, (5) graphite ribbon. ^b As determined using XANES. ^c As reported by the supplier.

X-ray beam incident at an angle of $\sim 45^\circ$ to the sample normal to take into account the \cos^2 angular dependence of the π^* resonance intensity.³²

JEOL 2010F field emission TEM operating at accelerating voltages of 100 and 200 kV was used for high-resolution imaging of ND particles. To minimize the in situ transformation of diamond to graphitic carbon under the electron beam, exposure of ND samples to the electron beam was limited to 5 and 1 min for 100 and 200 kV, respectively. TEM samples were prepared by dispersing ND in isopropyl alcohol over a copper grid coated with a lacey carbon film.

Fourier transform infrared (FTIR) spectra were collected using a Digilab FTIR spectrometer equipped with a Digilab UMA 600 microscope evading any sample preparation for the measurements.

- (23) Landi, B. J.; Cress, C. D.; Evans, C. M.; Raffaella, R. P. *Chem. Mater.* **2005**, *17*, 6819–6834.
- (24) Park, T. J.; Banerjee, S.; Hemraj-Benny, T.; Wong, S. S. *J. Mater. Chem.* **2006**, *16*, 141–154.
- (25) Xu, X. Y.; Li, X. G. *Chin. Chem. Lett.* **2005**, *16*, 249–252.
- (26) Aleksenskii, A. E.; Baidakova, M. V.; Vul, A. Y.; Siklitskii, V. I. *Phys. Solid State* **1999**, *41*, 668–671.
- (27) Brenner, D. W.; Shenderova, O. A.; Areshkin, D. A.; Schall, J. D.; Frankland, S. J. V. *CMES: Comput. Model. Eng. Sci.* **2002**, *3*, 643–673.
- (28) Ferrari, A. C.; Robertson, J. *Philos. Trans. R. Soc. London, Ser. A* **2004**, *362*, 2477–2512.
- (29) Reich, S.; Thomsen, C. *Philos. Trans. R. Soc. London, Ser. A* **2004**, *362*, 2271–2288.
- (30) Praver, S.; Nemanich, R. J. *Philos. Trans. R. Soc. London, Ser. A* **2004**, *362*, 2477–2512.
- (31) Praver, S.; Nugent, K. W.; Jamieson, D. N.; Orwa, J. O.; Bursill, L. A.; Peng, J. L. *Chem. Phys. Lett.* **2000**, *332*, 93–97.
- (32) Stöhr, J. *NEXAFS Spectroscopy*; Springer: Berlin, 2003.

Results and Discussion

Thermogravimetric Analysis. To determine the appropriate temperature range for the selective oxidation of nondiamond carbon, nonisothermal TGA was performed in air. Figure 1a compares the oxidation behavior of the ND samples and shows differences in the oxidation rate and the temperature at which the maximum weight loss occurs. At temperatures below 375 °C, the oxidation is inhibited or its rate is too low to allow noticeable removal of carbon within a reasonable time frame (range I). At temperatures above 450 °C, all kinds of carbon in the sample, including amorphous, graphitic, and diamond phases, are quickly oxidized (range III). In the intermediate temperature zone (range II), the oxidation rate shows substantial differences between the samples: while the mass of relatively pure UD98 does not change noticeably, UD50 with a substantial graphitic content (Table 1) shows a significant weight loss.

Metal and metal oxide impurities present in all ND samples also affect TGA results and account for a noticeable difference in the oxidation of UD90 and UD98 (Figure 1a), which have similar contents of sp²-bonded carbon (Table 1) but show some variation in the level of non-carbon impurities. To confirm the effect of iron on the oxidation kinetics of carbon, we performed TGA analysis of metal-free nanosized amorphous carbon black

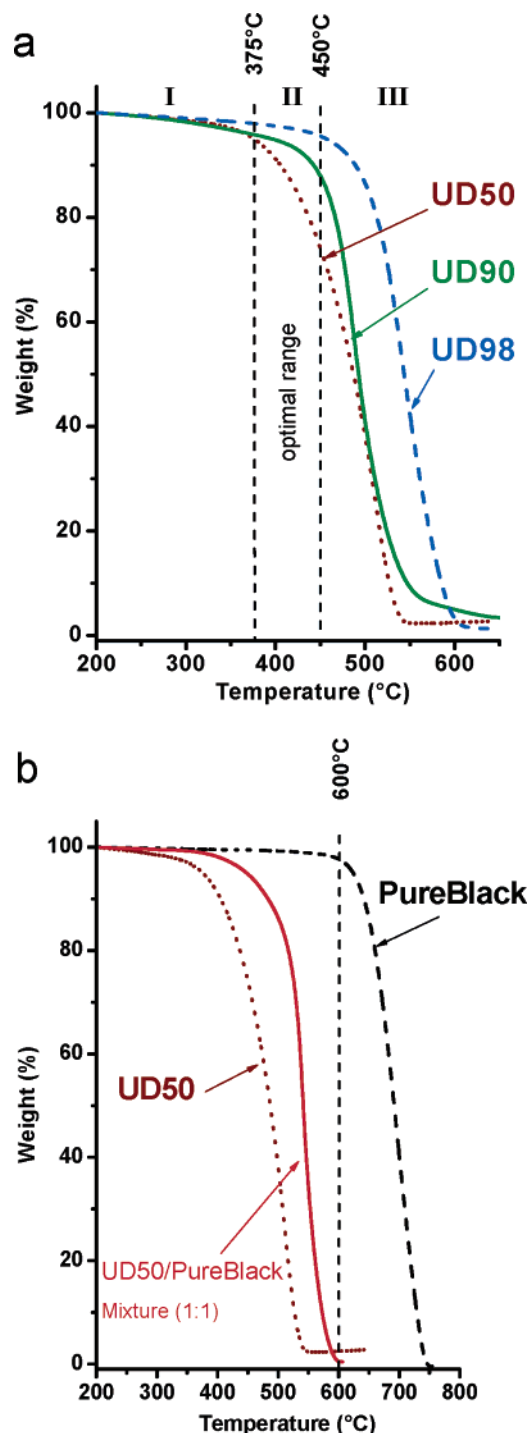


Figure 1. Nonisothermal TGA of ND samples (a) and carbon black powder (PureBlack), UD50, and their mixture (b) in air. The graphs are normalized by the sample weight at 200 °C, the temperature at which physisorbed water and organic impurities are mostly removed from the diamond surface, but the oxidation of carbon does not occur.

powder (PureBlack) with and without an addition of UD50 in the mixture (1:1) (Figure 1b). PureBlack alone demonstrated resistance to oxidation at temperatures below ~ 600 °C. However, the mixed powder was fully oxidized before even reaching 600 °C. Iron particles, the major contaminants of ND, are well-known for their catalytic behavior toward reactions between molecular oxygen and carbon.^{23–25} Metals and metal oxides encapsulated into amorphous and graphitic carbon shells in as-produced soot could become accessible to liquid oxidizers only

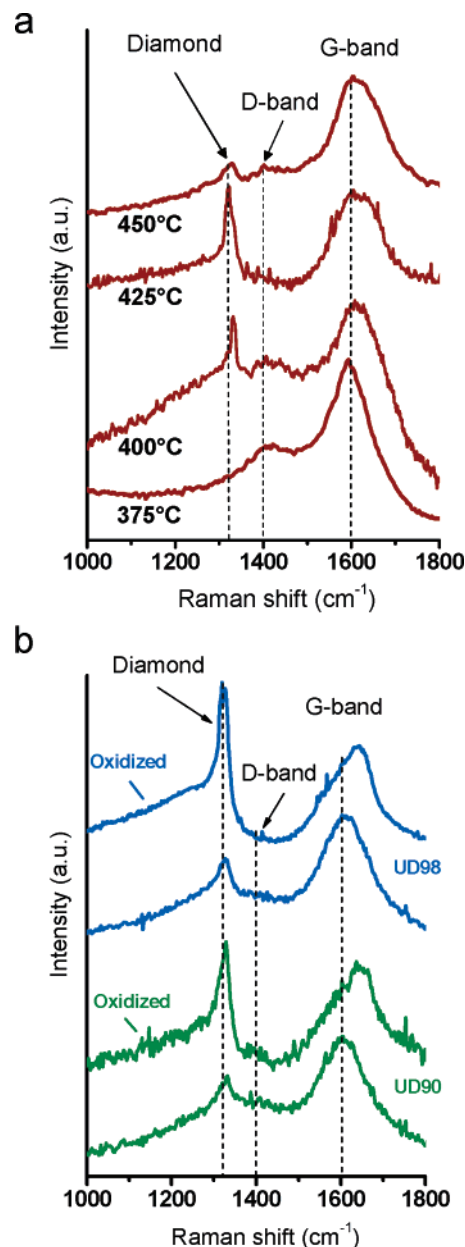


Figure 2. UV (325 nm) Raman spectra of UD50 after oxidation at 375, 400, 425, and 450 °C for 5 h in air (a) and comparison of UD90/UD98 before and after oxidation for 5 h at 425 °C (b). A substantial enhancement of the diamond band after oxidation is evident for all ND samples and is due to removal of graphitic carbon.

after carbon shells are removed by preceding acid treatments.^{3,26,27} The limited efficiency of wet chemistry in removing sp^2 carbon thus strongly affects the removal of non-carbon impurities and emphasizes the importance of using alternative purification techniques.

UV Raman Spectroscopy. To determine the optimal oxidation temperature and time, we oxidized ND for 5 h at different temperatures between 375 and 450 °C with 10–15 °C steps and characterized the samples using UV–Raman spectroscopy. Figure 2a shows results for UD50. The raw unpurified powder was chosen because of its large content of nondiamond carbon and more evident spectral changes. The UV–Raman spectrum of ND shows three characteristic features: the disorder-induced double-resonance D band at ~ 1400 cm^{-1} ,^{28,29} the upshifted graphite G band at 1600 cm^{-1} ,^{28,29} and the downshifted and

broadened, with respect to the Raman mode of single-crystal diamond (1332 cm⁻¹), diamond peak at ~1325 cm⁻¹ 20,30,31 (Figure 2a). The lower oxidation temperature (375 °C) was not sufficient to remove amorphous and graphitic carbon. Because of the much larger Raman scattering cross section of graphite compared to that of diamond, the Raman spectrum is dominated by the Raman features of sp²-bonded carbon (D and G bands), which overshadow the diamond band. Fullerenic shells enclose the diamond crystals and further weaken their Raman signal. At temperatures above 450 °C, oxidized powders become inhomogeneous with respect to the ratio of diamond and nondiamond carbon phases. The Raman intensities of the diamond peak at ~1325 cm⁻¹ and G-band at ~1600 cm⁻¹ vary strongly when comparing the UV Raman spectra recorded at different sample spots (data not shown), suggesting that all types of carbon are oxidized simultaneously leading to an inhomogeneous diamond distribution. When using oxidation temperatures between the extremes (375–450 °C), nondiamond carbon can be removed selectively and a significant loss of the diamond can be avoided. The Raman spectrum of the UD50 oxidized at 400 °C demonstrates a substantially enhanced diamond signal. The intensity ratio between the diamond band and the G band in the Raman spectrum of ND reaches a maximum within this temperature range, indicating the best conditions for the ND purification, which maximize the diamond content and minimize the amount of both amorphous and graphitic carbon.

In situ Raman spectroscopy was used for the improvement of the purification process (data not shown). While the optimal oxidation temperature could be affected by both the sample composition and the experimental conditions, temperatures within the 400–430 °C range were found to be most favorable in the present study. Small changes in the oxidation temperature within the given range can be used to find a compromise between the higher purification rate (lower time and costs) and the acceptable weight loss due to minor oxidation of the diamond phase.

The determined oxidation conditions were then used to purify larger amounts of ND in a chamber furnace to simulate industrial conditions. The weight loss in these experiments was very close to the amount of sp² carbon in the samples (Table 1). Figure 2b compares the UV–Raman spectra of the as-received and the purified by 5-h oxidation at 425 °C ND samples. The Raman spectra of the as-received UD90 and UD98 show a lower intensity of D-band as compared to UD50 and presence of a nanodiamond peak. The oxidation leads to a significant increase in the relative intensity of the diamond peak in all the samples, the most dramatic changes being observed in UD50 (Figure 2a). While air oxidation evidently removes fullerenic shells and other sp²-bonded carbon impurities from the samples, it also influences the surface chemistry and thus affects the shape of the Raman peaks. The appearance of a shoulder at 1140–1300 cm⁻¹ as well as the strong upshift of the G peak to ~1640 cm⁻¹ in the oxidized samples could be the manifestations of bond formation of carbonyl oxygen containing functional groups (e.g., ketone) on sp²- or sp³-bonded carbon.²⁸ A similar upshift of the G band was also observed in disordered diamond-like carbon (also called tetrahedral carbon) with a high content of sp³-bonded carbon and explained by resonance phenomena.²⁸ However, we believe that since ND surface atoms account for more than 20% of total atoms in ND particles below 5 nm, surface functionalities are

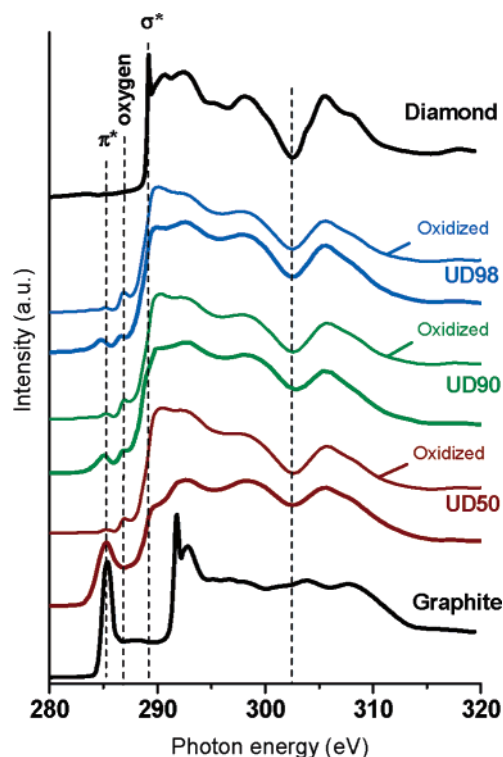


Figure 3. C K-edge XANES spectra of UD50, UD90, and UD98 before and after oxidation for 5 h at 425 °C in air. Reference XANES spectra of microcrystalline diamond and highly ordered pyrolytic graphite (HOPG) are shown for comparison. Substantial decrease in the intensity of 1s → π^* peak at ~284.5 eV and correspondingly lower content of sp² carbon in oxidized ND is evident.

responsible for this peak and a FTIR confirmation of this statement will be presented below.

X-ray Absorption Near-Edge Structure Spectroscopy. XANES allowed us to quantify the sp³ content in ND samples and learn about their bonding structure. As compared to electron energy loss spectroscopy, XANES is a more quantitative technique that offers a better spectral resolution, minimizes the sample damage, and allows one to obtain an averaged signal from a macroscopic sample. The C K-edge XANES spectra reflect angular-momentum-selected electronic transitions from the C 1s core level into the conduction band. Hence, if possible core–hole relaxation and electron correlation effects and higher multipole transitions are ignored, XANES spectra map the p-projected density of empty C-related states above the Fermi level.³²

Figure 3 compares the XANES spectra of graphite, microcrystalline diamond, and all the ND samples before and after oxidation in air. The spectra of ND exhibit two peaks centered at ~285.4 and ~286.5 eV and a broad band absorption with a threshold at ~289 eV. The peak at ~285.4 eV is assigned to the 1s → π^* transition of sp²-bonded carbon,³² while the ~286.5 eV peak can be related to the chemisorbed oxygen (C=O).^{32,33} Our assignment of this peak is also supported by the correlation of its relative intensity with the intensity of peaks in the second-order O K-edge at ~272 eV (not shown). The broad peak with an absorption edge at ~289 eV is related to the 1s → σ^* transitions. Diamond lacks π^* states and shows an absorption edge at 289 eV (1s → σ^* of sp³-bonded C), while graphite shows

(33) Jaouen, M.; Tourillon, G.; Delafond, J.; Junqua, N.; Hug, G. *Diamond Relat. Mater.* **1995**, *4*, 200–206.

Table 2. Results of the sp^2/sp^3 Content Analysis of ND Samples by XANES before and after 5-h Oxidation at 425 °C in Air^a

	HOPG	microcrystalline diamond	UD50		UD90		UD98	
			as-received	oxidized	as-received	oxidized	as-received	oxidized
sp^3 content, %	0	98	23	95	70	94	81	96
sp^2 content, %	100	2	77	5	30	6	19	4
sp^3/sp^2 ratio	0	49	0.3	19	2.3	16	4.3	24

^a Data obtained on a reference microcrystalline diamond powder and HOPG are shown for comparison.

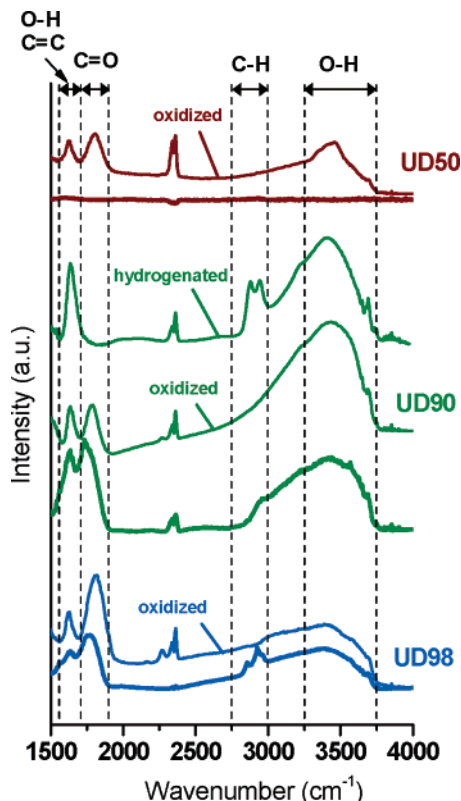


Figure 4. FTIR spectra of UD50, UD90, and UD98 samples before and after oxidation for 5 h at 425 °C in air. A spectrum of oxidized UD90 that was annealed for 2 h at 800 °C in hydrogen (20 mL/min) is shown to demonstrate the possibility to control the surface chemistry of ND after oxidation.

two absorption edges at 284 eV ($1s \rightarrow \pi^*$) and 291 eV ($1s \rightarrow \sigma^*$ of sp^2 -bonded C). The oxidation treatment of ND samples resulted in the substantial decrease of $1s \rightarrow \pi^*$ related transitions and a more pronounced second band gap dip of diamond at ~ 302.5 eV, confirming the Raman studies previously discussed. Some increase in the oxygen-related peak intensities was also observed. The results of the semiquantitative analysis of sp^3 -bonded carbon content in ND samples are presented in Table 2. Not only did oxidation in air decrease by about five times sp^2 -bonded carbon impurities in the ND (UD90 and UD98) samples prepurified by acidic treatment, but also it was capable of selectively removing graphitic carbon in the soot sample (UD50), thus increasing the sp^3/sp^2 ratio in this sample by nearly 2 orders of magnitude from 0.3 to 19 (Table 2). The purity of the oxidized UD98 is comparable to that of microcrystalline diamond. While some authors claimed a high content ($>92\%$) of diamond in the ND powders, those conclusions were based on X-ray photoelectron spectroscopy and X-ray diffraction (XRD) measurements of the diamond/graphite ratio³⁴ and cannot

(34) Huang, F.; Tong, Y.; Yun, S. *Phys. Solid State* **2004**, *46*, 616–619.

be considered reliable, because XRD overestimates the diamond content and surface analysis techniques cannot provide good quantitative data for powdered materials. To the best of our knowledge, $>95\%$ sp^3 carbon has never been found in ND samples by XANES or nuclear magnetic resonance spectroscopy.

Fourier Transform Infrared Spectroscopy. While XANES analysis is useful to distinguish between the different carbon species, FTIR spectroscopy was used to determine functional groups, adsorbed molecules, and impurities on the surface of the carbon. The main features in the FTIR spectra of as-received powders (Figure 4) are related to C=O ($1740\text{--}1757\text{ cm}^{-1}$), C–H ($2853\text{--}2962\text{ cm}^{-1}$), and O–H vibrations ($3280\text{--}3675\text{ cm}^{-1}$ stretch and $1640\text{--}1660\text{ cm}^{-1}$ bend), which can be assigned to $-\text{COOH}$, $-\text{CH}_2-$, $-\text{CH}_3$, and $-\text{OH}$ groups of chemically bonded and adsorbed surface species.^{35–37} Black and strongly absorbing as-received UD50 shows no detectable FTIR vibrations due to the high content of graphitic and amorphous carbon structures. The comparison of FTIR spectra of purified and as-received powders reflects the conversion of a variety of surface functional groups into their oxidized derivatives. After oxidation, $-\text{CH}_2-$ and $-\text{CH}_3$ groups are completely removed from UD90 and UD98, the amount of $-\text{OH}$ groups is increased, and C=O vibrations are upshifted by $20\text{--}40\text{ cm}^{-1}$, indicating a conversion of ketones, aldehydes, and esters on the surface into carboxylic acids, anhydrides, or cyclic ketones. The most prominent changes in the surface termination after oxidation were found for UD50. Upon the removal of graphitic layers by oxidation, the surface of UD50 becomes accessible for chemical reactions and is immediately saturated with oxygen or oxygen-containing functional groups. The oxidized ND with controlled surface is thus ready for further modifications and functionalization procedures. We have demonstrated this by hydrogenating oxidized UD90 for 2 h in a hydrogen gas flow of 20 mL/min at 800 °C. This led to complete disappearance of C=O vibrations in the FTIR spectrum (Figure 4), a drastic decrease of the oxygen peak in the XANES spectrum, and an increase in the intensity of C–H vibrations in the FTIR spectrum, suggesting formation of hydrogen-terminated ND. The hydrogenated sample is better dispersed in nonpolar solvents, such as toluene, while the oxidized sample could be easily dispersed in water and alcohols, but immediately precipitates on the bottom of the vial in nonpolar hydrocarbon solvents.

Transmission Electron Microscopy. TEM studies fully support results of Raman and XANES analyses, showing elimination of graphitic ribbons, carbon onions, and graphitic shells in UD50 and a substantial decrease in amorphous carbon

(35) Ji, S. F.; Jiang, T. L.; Xu, K.; Li, S. B. *Appl. Surf. Sci.* **1998**, *133*, 231–238.

(36) Jiang, T.; Xu, K. *Carbon* **1995**, *33*, 1663–1671.

(37) Kuznetsov, V. L.; Aleksandrov, M. N.; Zagoruiko, I. V.; Chuvilin, A. L.; Moroz, E. M.; Kolomichuk, V. N.; Likholobov, V. A.; Brylyakov, P. M.; Sakovitch, G. V. *Carbon* **1991**, *29*, 665–668.

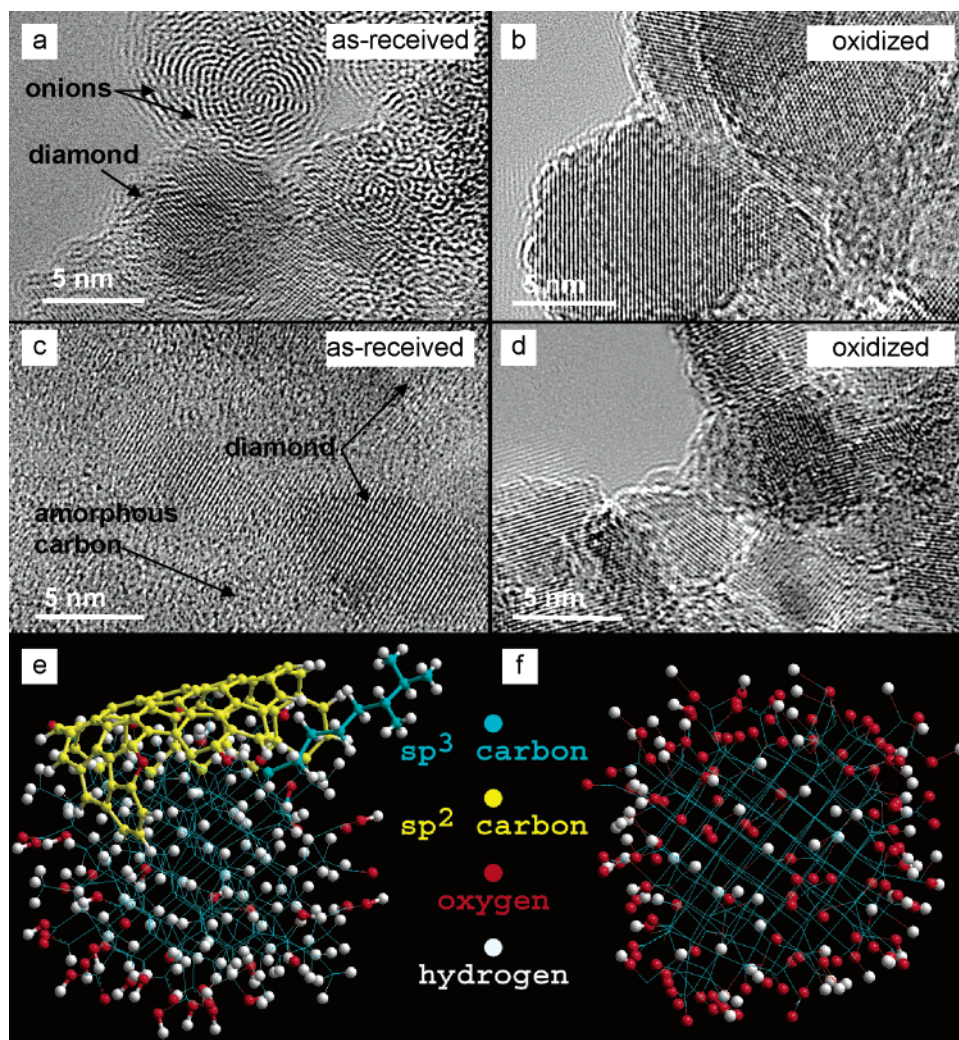


Figure 5. HRTEM images of (a, b) UD50 and (c, d) UD90 before and after oxidation for 5 h at 425 °C in air. HyperChem models of ND (e) before and (f) after oxidation.

content in UD90 and UD98 after oxidation. Figure 5 shows representative high-resolution micrographs of UD50 and UD90 before and after annealing in air. The microstructure of UD98 was very similar to that of UD90 and thus is not presented separately. This is in agreement with XANES measurements showing a similar sp²/sp³ carbon ratio for these grades before and after oxidation. Interestingly, the oxidation also decreased the degree of aggregation in ND samples. Prior to oxidation, no isolated diamond nanoparticles could be observed in TEM; they were always agglomerated. However, once oxidized, numerous single ND particles covered the lacey carbon on the TEM grid (Figure 6). While agglomeration of nanoparticles depends on surface charge, chemistry, pH of the solution, and other parameters, our observation indicates that oxidation removed the sp² carbon that bridged the diamond particles into clusters^{3,5} in the as-produced or acid-purified ND. Once sp² carbon or other bridges in ND clusters are removed, dispersion of ND to single particles becomes feasible. This is extremely important in many applications of ND.

The HyperChem models of ND particles (Figure 5e,f) summarize results of FTIR, XANES, Raman, and TEM analyses. They show that a rather complex surface chemistry of initial diamond with graphite, hydrocarbons, and oxygen-containing groups covering the surface becomes cleaner and more uniform

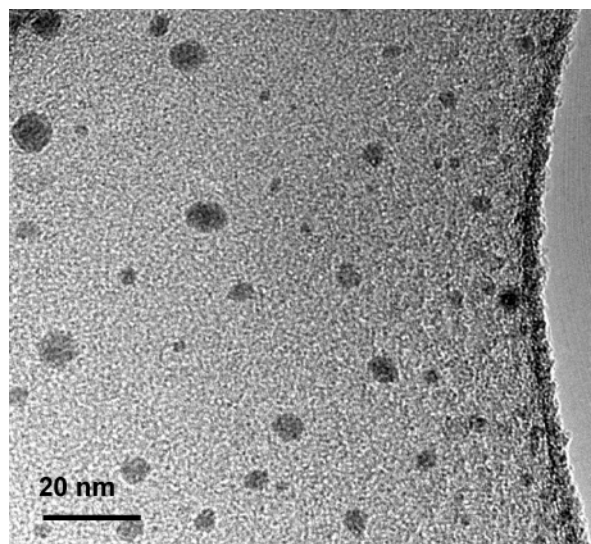


Figure 6. Low-resolution TEM image of nanodiamond particles of the oxidized UD90 on a lacey carbon film.

and has a higher concentration of reactive oxygen-containing moieties attached.

Optical Imaging. Visual analysis of dry ND suggests substantial improvement in its technological properties after

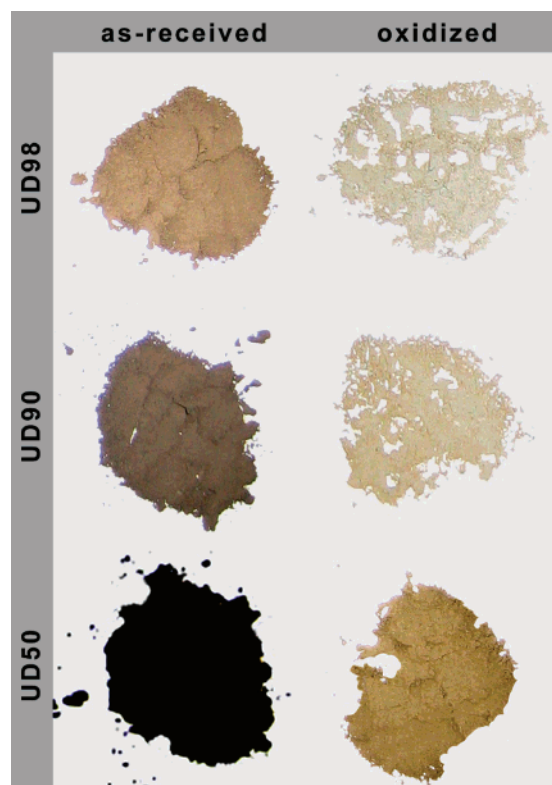


Figure 7. Optical images of UD50, UD90, and UD98 before and after oxidation for 5 h at 425 °C in air.

oxidation. The oxidized powder in the vials shows a liquidlike behavior when shaken, and flows easily, probably due to particle separation and breaking of agglomerates (Figure 6). Figure 7 shows optical images of the as-received and the oxidized ND. In general, the darkness of powders correlates quite well with the content of sp^2 -bonded carbon and other impurities in the samples (compare Figure 7 with Tables 1 and 2). Untreated UD50 appears velvet black. UD90 and UD98 look gray (UD90) or gray-brown (UD98). While all the purified samples appear light gray in color, the oxidized UD98 looks very similar to microcrystalline diamond powder, confirming its high purity. Transparency of ND could be important for many potential applications in scratch-resistant optics, windows, and displays. Removal of graphitic carbon is also expected to decrease the electrical conductivity of the powders. High electrical resistivity and high thermal conductivity of diamond may allow the use of ND in heat management as an additive to polymers. Due to the reduced level of impurities, the high diamond content, and the uniform oxygen-bearing surface terminations, oxidized nanodiamond can be considered as the most appropriate starting

material for further wet chemistry modification and biomedical applications. The simplicity and environmental friendliness of this single-step process should make it well-accepted in both industrial and research environments.

Conclusions

Our studies demonstrate the possibility of selectively removing amorphous and graphitic sp^2 -bonded carbon from nanodiamond powders by oxidation in air. The optimal temperature range for oxidation of the ND samples investigated is 400–430 °C. Depending on the ND sample, 5-h oxidation at 425 °C increased the content of sp^3 -bonded carbon from 23 to 81% in starting powders to 94–96%, as determined by XANES, and the weight loss was roughly equal to the content of sp^2 carbon in the sample. The purity of ND thus became comparable to that of microcrystalline diamond. Metal impurities, which were initially protected by carbon shells in the as-received samples, become accessible after oxidation and can be completely removed by further treatment in diluted acids. FTIR spectroscopy revealed that oxidation results in nanoparticles covered by oxygen-containing functional groups such as C=O, COOH, and OH. Carbonyl and carboxyl groups can be completely eliminated by subsequent hydrogenation at elevated temperatures.

These findings demonstrate the use of ambient air for the oxidative purification of diamond-bearing detonation soot, eliminating the need for any additional oxidizers, catalysts, or inhibitors. Moreover, the presented technique is also capable of significantly improving the quality of diamond samples which underwent prior acid purification treatments without appreciable loss of the diamond phase. These results open avenues for numerous new applications of nanodiamond.

Acknowledgment. We are grateful to Prof. C. Y. Li for providing access to the thermobalance and Kris Behler for experimental help (both at Drexel University). This work was partially supported by NanoBlox, Inc. The Renishaw 1000/2000 Raman spectrometer was purchased with an NSF grant (DMR-0116645) and is supported and managed by the Centralized Materials Characterization Facility of the A. J. Drexel Nanotechnology Institute. TEM studies were performed at Penn Regional Nanotechnology Facility. Work at LLNL was done under the auspices of the U.S. DOE by the University of California, LLNL under Contract No. W-7405-Eng-48. The ALS is supported by the Director, Office of Science, Office of BES, Materials Sciences Division, of the U.S. DOE under Contract No. DE-AC03-76SF00098 at LBNL. S.O. is supported by Arkema PhD Fellowship.

JA063303N